Available online at www.sciencedirect.com
ScienceDirect
Ceramics International 37 (2011) 1681–1688
CERAMICS INTERNATIONAL
www.elsevier.com/locate/ceramint

Sintering of Al_2O_3–SiC composite from sol–gel method with MgO, TiO_2 and Y_2O_3 addition

R. Mohammad-Rahimi [a], H.R. Rezaie [b,*], A. Nemati [c]

[a] Department of Materials Engineering, Islamic Azad University, Science and Research Branch, Tehran, Iran
[b] Department of Metallurgical and Materials Engineering, Iran University of Science and Technology (IUST), Tehran, Iran
[c] Department of Material Science Engineering, Sharif University of Technology, Tehran, Iran

Received 20 September 2010; received in revised form 19 December 2010; accepted 24 January 2011
Available online 18 February 2011

Abstract

Al_2O_3–SiC composite ceramics were prepared by pressureless sintering with and without the addition of MgO, TiO_2 and Y_2O_3 as sintering aids. The effects of these compositional variables on final density and hardness were investigated. In the present article at first α-Al_2O_3 and β-SiC nano powders have been synthesized by sol–gel method separately by using $AlCl_3$, TEOS and saccharose as precursors. Pressureless sintering was carried out in nitrogen atmosphere at 1600 °C and 1630 °C. The addition of 5 vol.% SiC to Al_2O_3 hindered densification. In contrast, the addition of nano MgO and nano TiO_2 to Al_2O_3–5 vol.% SiC composites improved densification but Y_2O_3 did not have positive effect on sintering. Maximum density (97%) was achieved at 1630 °C. Vickers hardness was 17.7 GPa after sintering at 1630 °C. SEM revealed that the SiC particles were well distributed throughout the composite microstructures. The precursors and the resultant powders were characterized by XRD, STA and SEM.

Keywords: A. Sintering; B. Nanocomposites; D. Al_2O_3; D. SiC

1. Introduction

Early researchers found that second-phase particles have been effectively employed to reinforce alumina. Silicon carbide demonstrates attractive properties such as high modulus, high strength, good corrosion/oxidation resistance and good high-temperature strength [1–6].

Ceramics reinforced with SiC show better mechanical properties than their monolithic counterparts [7]. The addition of small volumes (5–10 vol.%) of a nano sized reinforcing SiC agent causes a significant improvement in the inherent mechanical properties of monolithic ceramics [8–16]. The mechanisms behind these observed improvements with these small additive volumes are not completely explained. It has been suggested that the SiC nano-particles restrict Al_2O_3 grain growth, and this is a main factor behind these improvements [15,16]. In addition the thermal expansion coefficient of alumina is much higher than silicon carbide and so the tensile stresses in the alumina matrix can facilitate crack propagating and, therefore, decrease its toughness. Meanwhile, the counter forces of particle compressive stresses can be passed to the grain boundaries and resulting in toughening. The change of grain and grain boundary toughness can, in turn, dramatically change the fracture behavior of the composites [17].

A composite ceramic requires a higher sintering temperature than a monolithic material. In addition, it may be necessary to apply an external pressure during densification in order to achieve a sufficiently high density. Therefore they have been densified by using hot pressing that is very expensive and it does also put restrictions on the sample geometry [8,11]. Pressureless sintering is another method for sintering composites but lack of pressure in it causes to obtain composites with lower density. Lack of pressure reduces the driving force for grain boundary movement. Consequently, in this situation reaching to high enough density is gained by using sintering aids [18,19].

From this point of view pressureless sintering is an interesting alternative for densification of composites green bodies. In general pressureless sintered Al_2O_3–SiC composites have been fabricated in temperatures between 1700 and 1900 °C with small additions of various metal oxides [25,26].

* Corresponding author. Tel.: +98 9121025394; fax: +98 2177240480.
E-mail address: hrezaie@iust.ac.ir (H.R. Rezaie).

0272-8842/$36.00
doi:10.1016/j.ceramint.2011.01.035

This paper presents a fabrication process for high dense pressureless sintered Al_2O_3–5 vol.% SiC composites. These samples were densified up to 97% with additions of MgO, TiO_2 at 1600 °C and 1630 °C. Energy dispersive spectroscopy (EDS) was performed on particles observed by scanning electron microscopy (SEM). The resulting microstructures were examined by the SEM and particular attention in observations was paid to the well distribution of SiC particles in matrix and also restriction from oxidation of SiC particles during sintering of composites. Vickers hardness was also determined and related to the microstructural properties.

2. Experimental procedures

The precursor solution for Al_2O_3 nano powder was prepared by sol–gel method using $AlCl_3$ anhydrous (Merck), distilled water and NH_4OH (Merck). At first, the aluminum chloride was mixed with distilled water. The solution was stirred using a magnetic stirrer at 25 °C for 1 h to obtain a transparent solution. Then NH_4OH was gradually added to the solution. The obtained gel was dried at 80 °C for 24 h. The dried gel was then ground and calcined at 1000 °C, 1100 °C and 1200 °C with the heating rate and soaking time of 10 °C/min and 2 h correspondingly.

The chemical reagents used for preparing saccharose–SiO_2 gel as β-SiC precursors were tetraethoxysilicate (TEOS $(C_2H_5)_4SiO_4$) (Merck) and saccharose ($C_{12}H_{22}O_{11}$) (Merck) as silicon and carbon source respectively. Ethanol (Merck) and distilled water were solvents and also oxalic acid (Merck) and ammonia (Merck) were catalysts. Firstly, tetraethylorthosilicate and ethanol were added into saccharose solution with the molar ratio of C/Si = 4/1. During the process of stirring for homogeneity, the pH value of the mixture was kept at 2–3 by using oxalic acid. After 4 h of stirring at room temperature ammonia was added and raised the pH up to 4.

The prepared dark brown gel was placed in drying oven at 100 °C for 24 h. The xerogel was ground and poured into a graphite crucible inside a sintering furnace and then fired at 1500 °C for 1 h in 0.1 MPa argon atmosphere for carbothermal reduction reactions with heating rate of 10 °C/min. Because of the existence of some residual carbon in obtained powders and probability of no desirable effect on final product, the prepared powders were fired at 700 °C in air atmosphere for 1 h to remove the extra carbon.

A powder mixture of nano α-Al_2O_3 and 4.1 wt.% nano SiC was milled by agate. Doped samples were also prepared by adding MgO, TiO_2, and Y_2O_3 (0.05–2 wt.% with respect to the Al_2O_3 content). The TiO_2 powder (Degussa, P-25), which is a standard material in the field of photocatalytic reactions, contains anatase and rutile phases in a ratio of about 3/1. Transmission electron microscopy showed that the anatase and rutile particles separately form their agglomerates. The average sizes of the anatase and rutile elementary particles are 85 and 25 nm, respectively. Table 1 demonstrates the MgO properties. Y_2O_3 nano powder was Merck production with the mean particle size of 50 nm. The experimental samples are shown in Table 2. To help green pallets formation 2 wt.% polyvinyl alcohol (PVA) was added. The mixed powders were uniaxially hand pressed at 137 MPa by using a small mold ($r = 1$, $h = 1$ cm). The green pallets were placed in an Al_2O_3 protective powder bed in an alumina crucible and pressureless sintered in nitrogen atmosphere with a flow rate of 5 l/min. Two different sintering temperatures, 1600 °C and 1630 °C, were applied. The heating rate was 10 °C/min and cooling at the same rate. The densities of the sintered samples were determined by using a technique based on Archimedes' principle with distilled water.

Table 1
The specification of MgO nano powder.

Ingredient name	Magnesium oxide
Empirical formula	MgO
Molecular weight	40.31 amu
Purity	≈99.9%
Average particle size	≈35 nm
Specific surface area	50 m^2/g
True density	3.60 g/m^3
Melting point	2850 °C
Boiling point	3600 °C

3. Results and discussion

3.1. Conditions for obtaining alumina nano powder

Aluminum chloride anhydrous was hydrolyzed in distilled water to produce the sol [20]. The initial pH of the sol should be fixed at 3–3.5. The hydroxides groups that were produced in this step finally linked together to form the gel at pH = 9. The appearance of the sol would be opaque or translucent when the ratio of NH_4OH/H_2O was lower than 0.2. Adding more NH_4OH would result in decreasing of the gelation time which may be attributed to the catalytic effect of it [21]. Generally, the gelation time decreases by increasing aluminum chloride due to increasing the rate of hydrolysis and condensation reactions. However, increasing the amount of aluminum content in the sol

Table 2
The experimental samples.

Material name	MgO (wt.%)	TiO_2 (wt.%)	Y_2O_3 (wt.%)	Sintering temperature (°C)	Density (%)	Hardness (GPa)	Matrix grain size(μm)
1	–	–	–	1600/1630 °C	93.9/94.1	14.1/13.3	–
2	2	–	–	1600/1630 °C	95.3/95.9	16.4	4
3	–	2	–	1600/1630 °C	95.1/96	16.8	2
4	2	2	–	1600/1630 °C	97.8/97.9	17.7	0.8
5	_	_	2	1600/1630 °C	95/95.5	15.2	4

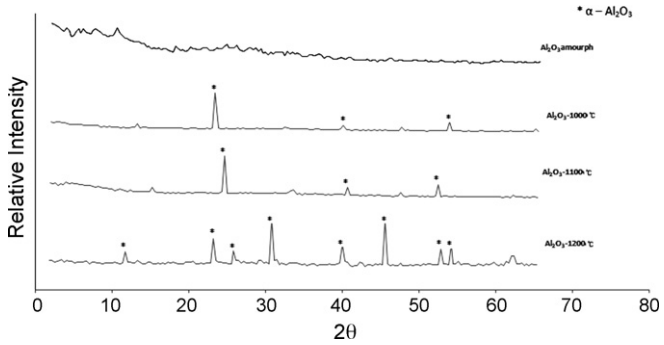

Fig. 1. The XRD patterns of the Al_2O_3 xerogel heat treated at various temperatures for 2 h.

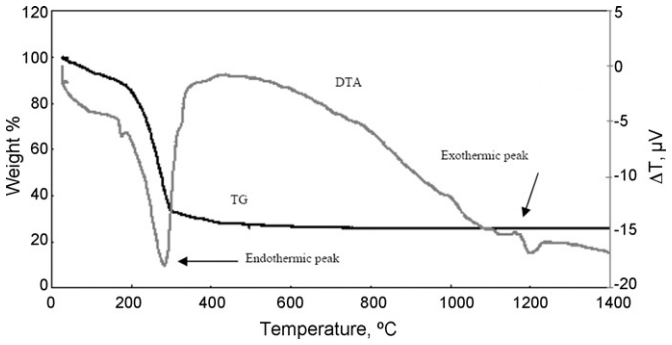

Fig. 2. The STA curve of alumina xerogel.

decreases transparency due to inadequate solubility of aluminum chloride in the sol. It seems an optimum ratio of NH_4OH/H_2O is 2. The first peaks of α-Al_2O_3 phase were detected in the gel heat treated at 1000 °C as can be seen in Fig. 1. By raising the temperature up to 1100 °C, the intensity of their corresponding peaks increases. Usually transformation of the metastable phases of alumina to the final stable α-alumina start at about 1100 °C but in this investigation α-Al_2O_3 was appeared at 1000 °C and completely crystallized at 1200 °C.

Fig. 2 shows the simultaneously thermal analyzer (STA) curve of the alumina xerogel. As shown in this figure 10% of weight loss of alumina xerogel was occurred at lower temperature than 200 °C and it is due to evaporation of volatile components. From 200 °C to 300 °C, the maximum weight lost was occurred due to the volatilization of chlorine which corresponds to two endothermic reactions. At 1200 °C, an exothermic reaction occurs due to transformation of transition phases of alumina to α-alumina [22].

Fig. 3 shows the microstructure of the α-Al_2O_3 powder after firing at 1200 °C. This figure shows the mean particle size of α-Al_2O_3 that heat treated at 1200 °C is about 200 nm and spherical in shape. The crystallite size calculations were done by using Scherreŕs equation resulted in 12.4 nm.

3.2. Conditions for obtaining silicon carbide nano powder

3.2.1. Conditions for obtaining gel

Oxalic acid and hydrolysis time are the two main factors that control the hydrolysis and gelation process. Both two parameters have the special optimum that deviation from these optimums causes negative effects on the xerogel and its characteristics. An increasing of temperature during hydrolysis process could accelerate reactions rate and so reducing the necessary hydrolysis time but in this article temperature was fixed to control the condition more precisely. After 4 h of stirring at room temperature and pH = 2–3, temperature was raised to 80 °C and ammonia gradually was added and increase the pH up to 5 and in this moment the initial nucleus were seen and after approximately 15 min the gel was obtained.

3.2.2. Mechanism of the sol–gel reactions

In the gel formation from TEOS, at first hydrolysis of Si–OC_2H_5 groups produced Si–OH groups. Then condensation between two Si–OH groups or between a Si–OH group and a Si–OC_2H_5 formed Si–O–Si chains. At the end the chains cross-link and/or entangle with each other in the whole liquid to form the gel [23]. It is proved that hydrolysis and condensation rates

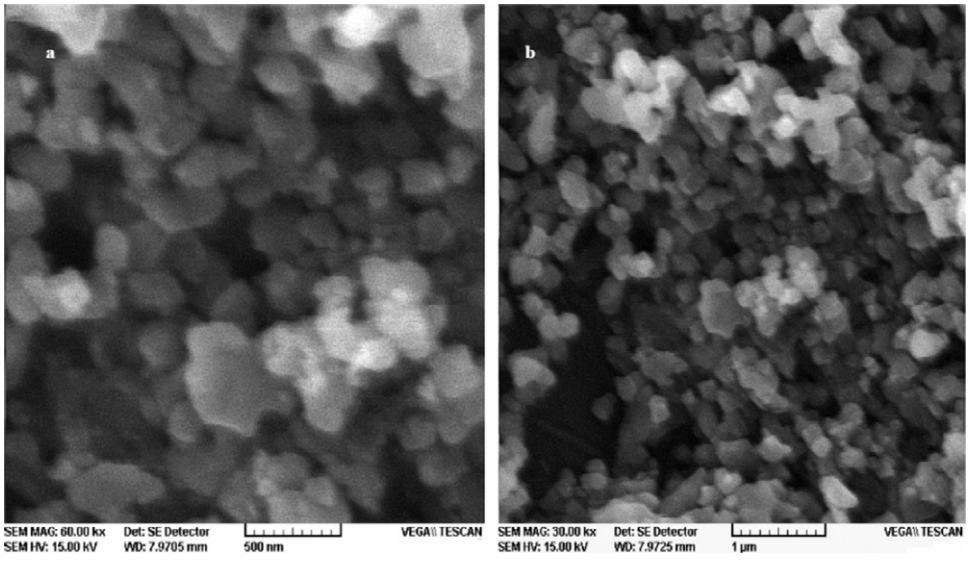

Fig. 3. The SEM images of α-Al_2O_3 nano powders at two magnitude (a) 6000 and (b) 3000.

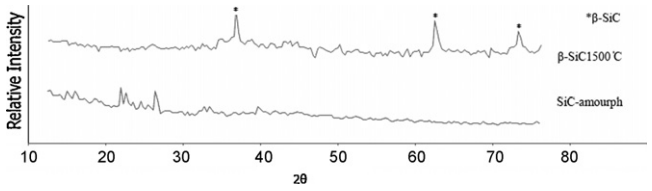

Fig. 4. The XRD patterns of the SiC xerogel heat treated at 1500 °C for 1 h.

of TEOS were greatly dependent upon the catalyst and the pH value. Typically when pH was below 7 hydrolysis rate increased with decreasing pH, but condensation rate decreased and reached its lowest point at pH = 2, the isoelectric point of silica [23].

3.2.3. Carbothermal reduction of the xerogel

For preparation of β-SiC powder, the dark brown dried gel should be reduced by carbothermal reduction. There are different reactions which may happen for producing the β-SiC but mostly silicon carbide can be formed by heterogeneous nucleation according to the following reaction [23]:

$$SiO(g) + C(g) \rightarrow SiC(s) + CO(g) \quad (1)$$

3.2.4. Characterization of the samples

XRD analysis presented in Fig. 4 showed that β-SiC is formed, and no other crystalline phases such as silica, carbon or other impurities are detected. This SiC has a well crystalline structure. The widths and intensities of the diffraction peaks in the XRD patterns are related to the average crystallite size, and they are often used to estimate the particle size [24]. According to Scherer's equation it was calculated that the crystallite size was 7.07 nm.

As shown in Fig. 5 for silica–saccharose xerogel, 10% of weight lost occurred in the range of 170–200 °C due to volatilize of water and volatile components such as alcohol. The maximum of weigh lost is 60% and is occurred in the range of 200–460 °C. Two endothermic peaks that are seen in this range confirm this point. Unfortunately this curve does not show any exothermic peak due to the phase transition of β-SiC. Phase transition of β-SiC needs high temperatures more than 1450 °C and the used STA equipment had temperature limitation.

The SEM images are shown in Fig. 6. It is seen that the sample mainly consists of irregular particles with mean particle

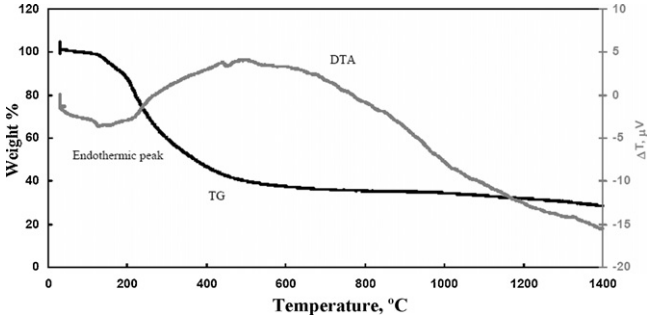

Fig. 5. The STA curve of SiO_2–saccharose xerogel.

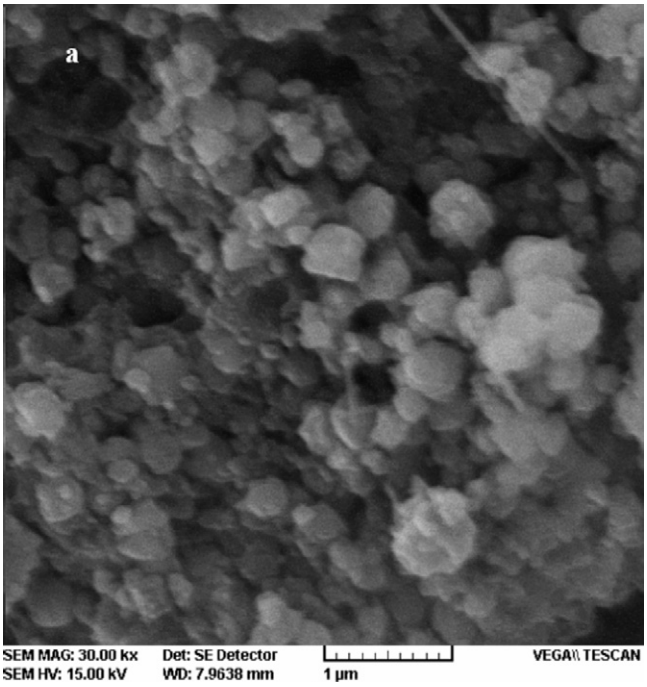

Fig. 6. The SEM images of SiC nano powder.

size of 250 nm. However, a few large particles were seen and this probably because of agglomerations of finer particles.

3.3. Microstructure of composites

There was a pronounced effect of MgO and TiO_2 additions on densification at 1600 °C and 1630 °C (see Table 2). Samples 2 and 3 that doped with MgO and TiO_2 reached 95.3% and 95.1% of full density at 1600 °C, while the undoped material (sample 1) only reached 93.9% at the same temperature. The effect of MgO and TiO_2 additions on density was less pronounced at the higher sintering temperature of 1630 °C. Sample 4 that consists of both MgO and TiO_2 simultaneously has the highest densities. The average matrix grain size increased at the higher sintering temperature. The smaller MgO and TiO_2 additions separately had, however, no pronounced effect on the grain size at any of the sintering temperatures but when they used together the average grain size was decreased (Table 2; Fig. 7). Only a limited number of larger grains were observed in the microstructures of the samples sintered at 1630 °C.

Sample 5 that consists of Y_2O_3 has the greatest mean grain size and the lowest density and hardness in both temperatures among other samples (Fig. 8).

Figs. 9 and 10 demonstrate the curves that compare samples density, hardness and mean grain size. As seen the smallest grain size belongs to sample 4. Grain boundaries and triple grain junctions in this sample were shown in Fig. 11. In this sample the highest density and hardness were achieved. Generally increasing hardness is along with increasing density.

In sample 1 (Fig. 12) without any sintering aids, the grains' shape was not changed while in the other samples the grains

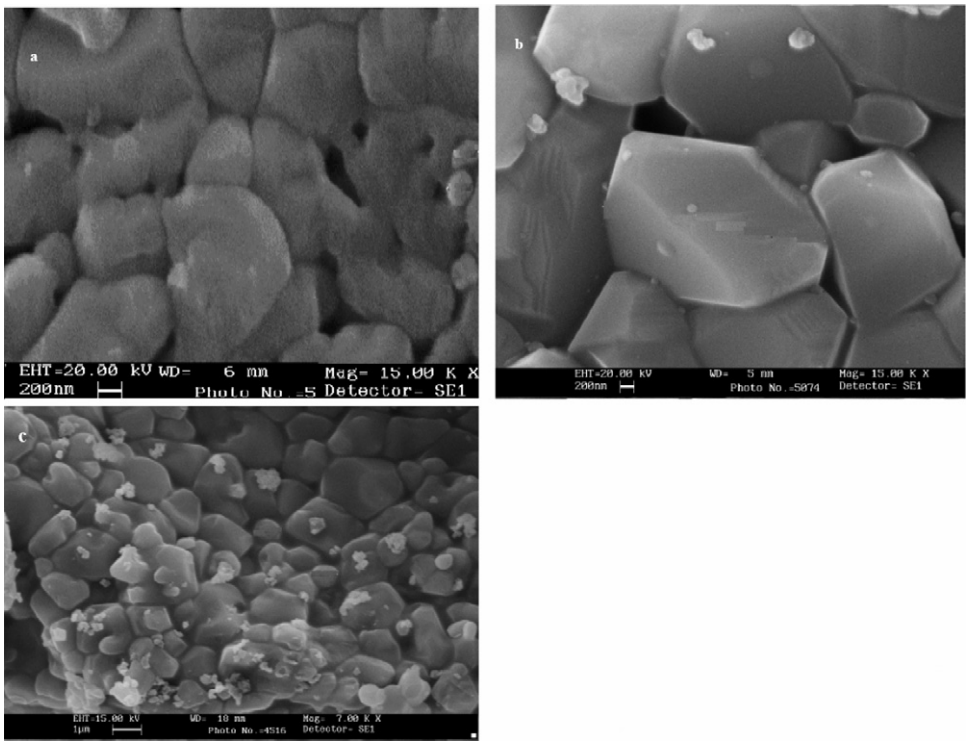

Fig. 7. Effect of (a) TiO_2, (b) MgO and (c) TiO_2 and MgO on grain size at 1630 °C.

shape were changed and they were almost multiangles. Comparing samples 2 and 3 resulted that TiO_2 was stronger in order to hinder grain growth than MgO (Fig. 7).

EDS point analysis and elemental distribution images computed from X-Ray Map (Fig. 13) suggested that the second phase particles were SiC. The small O-K_α peak and large C-K_α peak suggest that this is a SiC particle, with a small contribution from the Al_2O_3 matrix.

The SiC particles were well dispersed in the matrix, and located predominantly to the interiors of the Al_2O_3 matrix grains (Fig. 14).

From EDS analysis Ti-containing particles and Mg-containing particles were also found in materials with TiO_2 and MgO. Also N-containing particles were also found in most of the samples; these are likely to result from the N_2 sintering atmosphere used.

It is well demonstrated in the literature that a small additions (a few hundred ppm) of MgO is an effective densification aid during sintering of Al_2O_3 ceramics at temperatures in the range of 1600–1900 °C [25,26]. In this work separately and simultaneously the effect of MgO and TiO_2 were investigated. Additions of each of them have controlled the Al_2O_3 grain size by the Zener pinning [25–27]. Zener pinning is very important

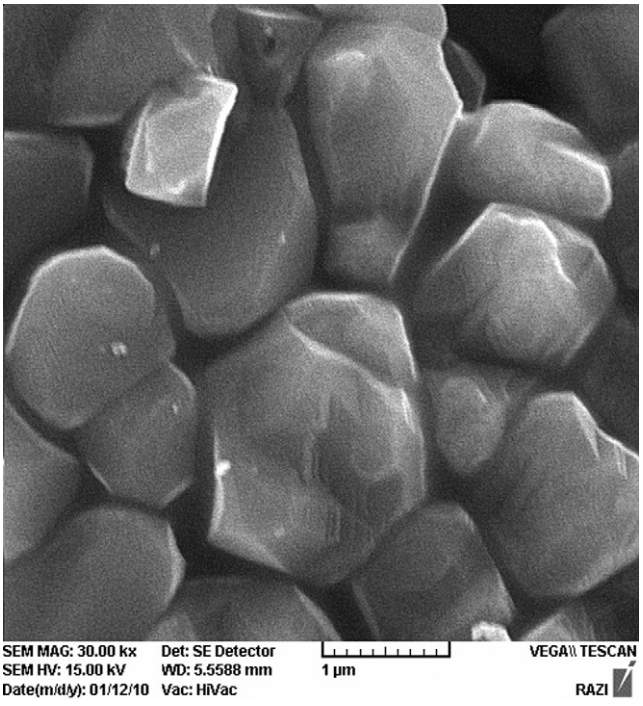

Fig. 8. Effect of Y_2O_3 on grain size at 1630 °C in sample 5.

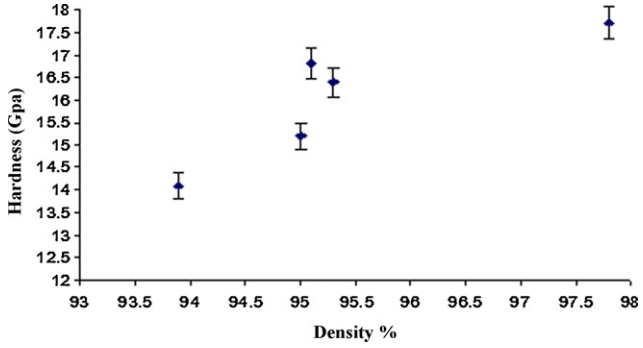

Fig. 9. Comparison of density with hardness in samples 1, 2, 3, 4 and 5.

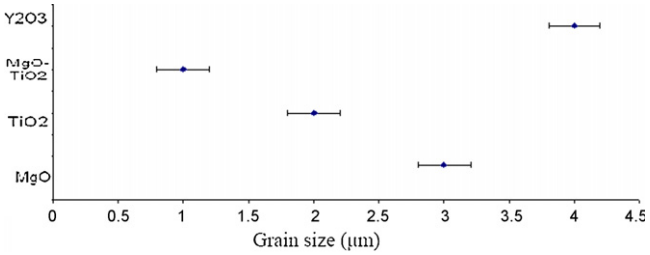

Fig. 10. Effect of sintering aids on grain size in samples 2, 3, 4 and 5.

in materials processing as it has a strong influence on recovery, recrystallization and grain growth. The smaller additions of MgO or TiO_2 in the samples in the present investigation did, however, not have any obvious effect on matrix grain size during sintering at a particular temperature (see Table 2). A limited number of large matrix grains were present also in the composites sintered with a smaller addition of MgO or TiO_2. This indicates that local abnormal grain growth did occur under the applied sintering conditions, despite the additions. MgO and TiO_2 may promote a more homogeneous grain size distribution by solute pinning of grain boundaries [27]. Other mechanisms that may operate in the presence of a glassy/liquid phase include modification of liquid–solid interfacial energies and glass viscosity [25]. Also by adding these sintering aids to this composite the significant segregation of Si, Mg and Ti in the grain boundaries would be occurred. Whether this causes a glassy grain boundary layer and in continues the segregation simply forms a boundary with a high diffusivity grain boundary layer. The much increased segregation in this material is presumably related to some interaction between SiC and TiO_2 or MgO. Such an interaction has previously been reported by Ding et al. [29] during the sintering of SiC. They found a much greater rate of oxidation of SiC in the presence of metal oxides such as Y_2O_3 and Al_2O_3 than they did when just Al_2O_3 was present. In this investigation the improvements can be

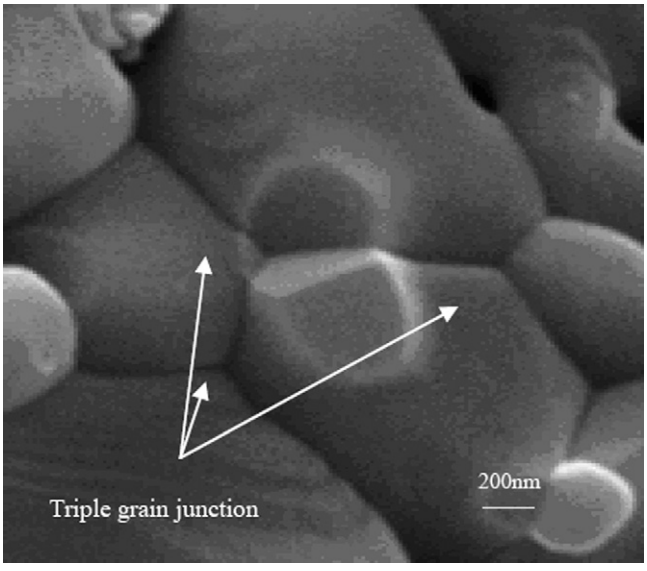

Fig. 11. Triple grain junction in sample 4.

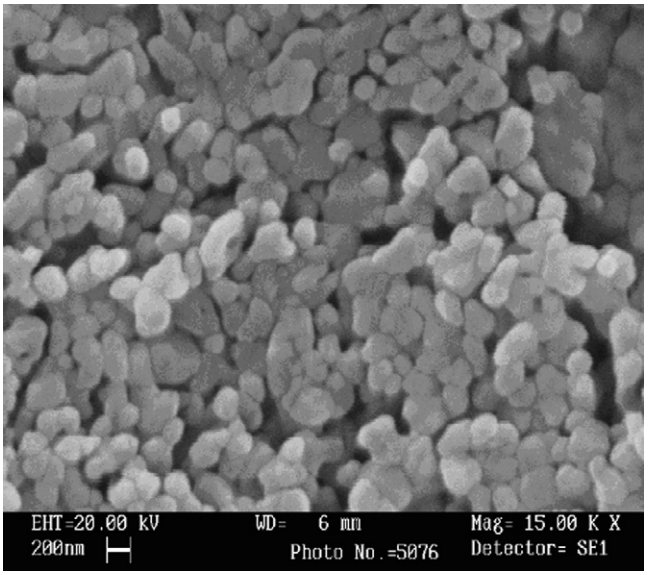

Fig. 12. Sample 1 without any sintering aids.

associated with the lower eutectic temperature of SiO_2–Al_2O_3–MgO (1355 °C) and SiO_2–Al_2O_3–TiO_2 (1470 °C) glassy phases compared to SiO_2–Al_2O_3 glass (1600 °C) [28]. The greater oxidation of SiC would release more SiO_2 which can contribute to the grain boundary glass or segregated layer, either of which may allow faster grain boundary diffusion.

In this investigation the samples with Y_2O_3 were the weakest samples not only in final densities but also in their microstructures. Improvement in sintering of Al_2O_3–SiC nanocomposites by adding Y_2O_3 has been previously observed [19,30,31]. Cock et al. [31] suggested that a glassy phase formed between SiO_2, Al_2O_3 and Y_2O_3 is responsible for this improvement. The lowest temperature eutectic between these compounds melts at 1371 °C [28]. Indeed, in temperatures less than this temperature Y_2O_3 inhibited sintering of the composite as same as it did in sintering of monolithic Al_2O_3. But as mentioned above in temperatures above the eutectic temperature there are some interactions between SiC and Y_2O_3 and this causes a much greater rate of oxidation of SiC and producing more SiO_2. This is consistent with Maclaren et al. [32] finding that SiO_2 and Y_2O_3 act in synergy to cause abnormal grain growth. They hypothesized that thin (<1 nm) disordered grain boundary layers, identified by HREM, were sufficient to trigger abnormal grain growth and decrease the mechanical properties and density. They attributed the disordered grain boundaries to the segregation of Si and Y concurrently.

3.3.1. Mechanical properties

Vickers hardness of the doped samples increased with density (see Table 2, Fig. 9). The sample without any additive had the lowest hardness of 14.1 GPa and 13.3 GPa respectively at 1600 °C and 1630 °C and the addition of 2 wt.% MgO and 2 wt.% TiO_2 resulted in a highest hardness of 17.7 GPa. The samples hardness that sintered at 1600 °C varied between 16.4 and 17.7 GPa (see Table 2).

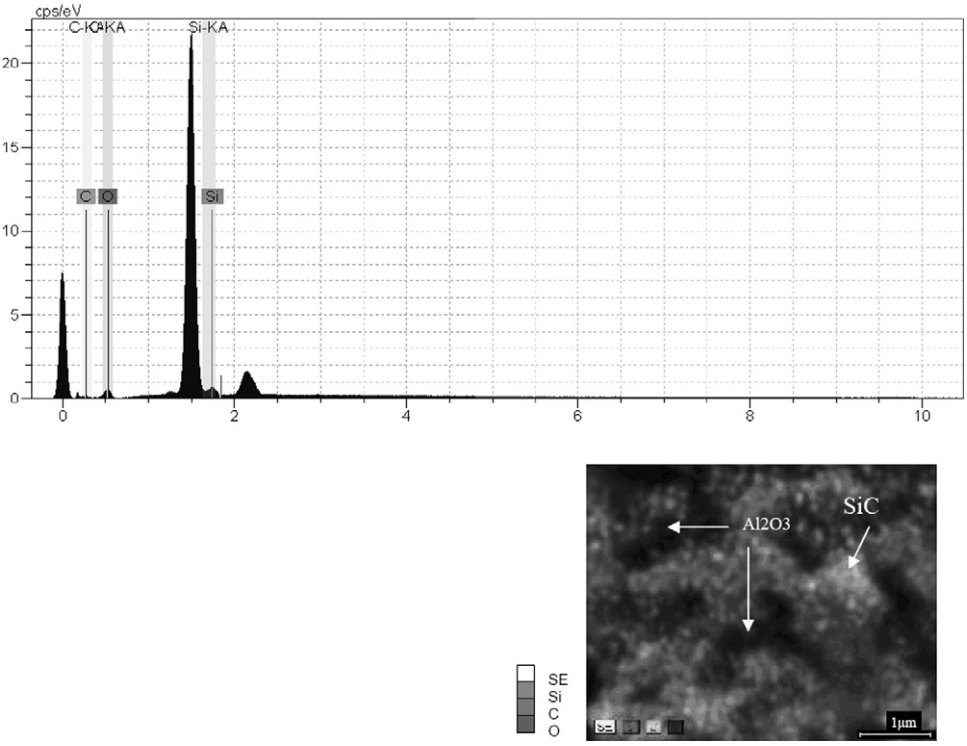

Fig. 13. EDS spectra of a Si-containing particle in sample 4.

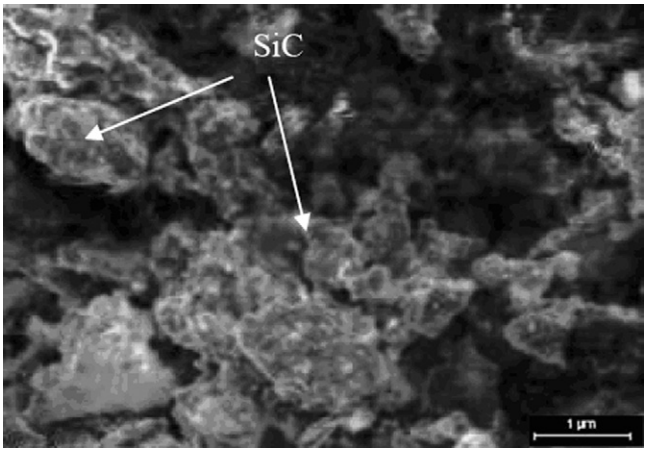

Fig. 14. X-ray map shows the SiC particles were dispersed homogenously in the matrix in sample 4.

4. Conclusion

α-Al_2O_3 and β-SiC submicron powders have been synthesized from aluminum chloride, TEOS and saccharose through the sol–gel route. The total weight loss of 60% appears in both gels after calcinations due to evaporation of volatile components. The Al_2O_3 nano powder with crystallite size of 12.4 nm and grains of 0.2 μm was formed after calcinations of the dried gel at 1200 °C. The particles were spherical in shape. β-SiC powder with a crystallite size of 7.07 nm and grains of 0.2 μm was obtained by carbothermal reduction of the xerogel in argon atmosphere at 1500 °C. Pressureless sintering of doped Al_2O_3–5 vol.% SiC composites to high density (97.9%) at comparatively lower temperature as usual (1600 °C and 1630 °C) was done. Additions of MgO and TiO_2 (2 wt.% with respect to the Al_2O_3) at the same time are most effective densification aids but Y_2O_3 had converse result on density and hardness .The SiC nanoparticles are well distributed and present at predominantly intragranular positions. Hardness is strongly dependent on density when the samples were sintered at 1630 °C.

References

[1] G. Magnani, A. Brillante, Effect of the composition and sintering process on mechanical properties and residual stresses in zirconia–alumina composites, J. Eur. Ceram. Soc. 25 (15) (2005) 3383–3392.
[2] J.O.L. Merino, R.I. Todd, Relationship between wear rate, surface pullout and microstructure during abrasive wear of alumina and alumina/SiC nanocomposites, Acta Mater. 53 (12) (2005) 3345–3357.
[3] M. Belmonte, M.I. Nieto, M.I. Osendi, P. Miranzo, Influence of the SiC grain size on the wear behavior of Al_2O_3/SiC composites, J. Eur. Ceram. Soc. 26 (7) (2006) 1273–1279.
[4] L.P. Ferroni, G. Pezzotti, Evidence for bulk residual stress strengthening in Al_2O_3/SiC nanocomposites, J. Am. Ceram. Soc. 85 (8) (2002) 2033–2038.
[5] X.D. Sun, J.G. Li, S.W. Guo, Z.M. Xiu, K. Duan, X.Z. Hu, Intragranular particle residual stress strengthening of Al_2O_3–SiC nanocomposites, J. Am. Ceram. Soc. 88 (6) (2005) 1536–1543.
[6] S. Taktak, M.S. Baspinar, Wear and friction behavior of alumina/mullite composite by sol–gel infiltration technique, Mater. Des. 26 (5) (2005) 459–464.
[7] Y.J. Lin, C.P. Tsang, The effect of starting precursors on the carbothermal synthesis of SiC powders, Ceram. Int. 29 (2003) 69–75.
[8] K. Niihara, New design concept of structural ceramics–ceramic nanocomposites, J. Ceram. Soc. Jpn. 99 (10) (1991) 974–982.
[9] T. Ohji, A. Nakahira, T. Hirano, K. Niihara, Tensile creep behavior of alumina/silicon carbide nanocomposite, J. Am. Ceram. Soc. 77 (12) (1994) 3259–3262.

[10] C.E. Borsa, N.M.R. Jones, R.J. Brook, R.I. Todd, Influence of processing on the microstructural development and flexure strength of Al_2O_3/SiC nanocomposites, J. Eur. Ceram. Soc. 17 (1997) 865–872.
[11] J. Perez-Rigueiro, J.Y. Pastor, J. Llorca, M. Elices, P. Miranzo, J.S. Moya, Revisiting the mechanical behavior of alumina/silicon carbide nanocomposites, Acta Mater. 46 (15) (1998) 5399–5411.
[12] A.J. Winn, R.I. Todd, Microstructural requirements for alumina–SiC nanocomposites, Br. Ceram. Trans. 98 (5) (1999) 219–224.
[13] D. Sciti, J. Vicens, A. Bellosi, Microstructure and properties of alumina–SiC nanocomposites prepared from ultrafine powders, J. Mater. Sci. 37 (2002) 3747–3758.
[14] A.M. Thompson, H.M. Chan, M.P. Harmer, Tensile creep of alumina/silicon carbide nanocomposite, J. Am. Ceram. Soc. 80 (9) (1997) 2221–2228.
[15] C.E. Borsa, S. Jiao, R.I. Todd, R.J. Brook, Processing and properties of Al_2O_3/SiC nanocomposites, J. Microsc. 177 (3) (1995) 305–312.
[16] M. Sternitzke, Review: structural ceramic nanocomposites, J. Eur. Ceram. Soc. 17 (1997) 1061–1082.
[17] F.C. Zhang, H.H. Luo, .S. Wang, M. Zhang, Y.N. Sun, Stress state and fracture behavior of alumina–mullite intragranular particulate composites, Compos. Sci. Technol. 68 (2008) 3245–3250.
[18] Y.K. Jeong, K. Niihara, Microstructure and mechanical properties of pressureless sintered Al_2O_3/SiC nanocomposites, Nanostruct. Mater. 9 (1997) 193–196.
[19] Y.K. Jeong, A. Nakahira, K. Niihara, Effects of additives on microstructure and properties of alumina–silicon carbide nanocomposites, J. Am. Ceram. Soc. 82 (12) (1999) 3609–3612.
[20] M.T. Chiou, Y. Tsai, Nanoscale deformation measurement by using the hybrid method of gray-level and holographic interferometry, J. Mater. Sci. 29 (1994) 2378–2388.
[21] M. Shojaie-Bahaabad, E. Taheri-Nassaj, R. Naghizadeh, An alumina–YAG nanostructured fiber prepared from an aqueous sol–gel precursor: preparation, rheological behavior and spinnability, Mater. Lett. 62 (2008) 3364–3366.
[22] A Sedaghat, E. Taheri-Nassaj, R. Naghizadeh, An alumina mat with a nano microstructure prepared by centrifugal spinning method, J. Non Cryst. Solid 352 (2006) 2818–2828.
[23] A.W. Weimer, K.J. Nilsen, G.A. Cochran, R.P. Roach, Kinetics of carbothermal reduction synthesis of beta silicon car-bide, AIChE Journal 39 (1993) 493–503.
[24] C.H. Dai, X.P. Zhang, J.S. Zhang, Y.J. Yang, L.H. Gao, Formation of double-side teethed nanocombs of ZnO and self-catalysis of Zn-terminated polar surface, J. Am. Ceram. Soc. 80 (5) (1997) 1274–1276.
[25] R.L. Coble, Sintering crystalline solids. II. Experimental test of diffusion models in powder compacts, J. Appl. Phys. 32 (5) (1961) 793–799.
[26] S.O. Bae, S. Baik, Critical concentration of MgO for the prevention of abnormal grain growth in alumina, J. Am. Ceram. Soc. 77 (10) (1994) 2499–2504.
[27] C.A. Bateman, S.J. Bennison, M.P. Harmer, Mechanism for the role of magnesia in the sintering of alumina containing small amounts of a liquid phase, J. Am. Ceram. Soc. 72 (7) (1989) 1241–1244.
[28] U. Kolitsch, H.J. Seifert, T. Ludwig, F. Aldinger, Phase equilibria and crystal chemistry in the Y_2O_3–Al_2O_3–SiO_2 system, J. Mater. Res. 14 (1999) 447–455.
[29] S.Q. Ding, S.M. Zhu, Y.P. Zeng, D.L. Jiang, Effect of Y_2O_3 addition on the properties of reaction-bonded porous SiC ceramics, Ceram. Int. 32 (2006) 461–466.
[30] S.K.C. Pillai, B. Baron, M.J. Pomeroy, S. Hampshire, Effect of oxide dopants on densification, microstructure and mechanical properties of alumina–silicon carbide nanocomposite ceramics prepared by pressureless sintering, J. Eur. Ceram. Soc. 24 (2004) 3317–3326.
[31] A.M. Cock, I.P. Shapiro, R.I. Todd, S.G. Roberts, Effects of yttrium on the sintering and microstructure of alumina–silicon carbide ''nanocomposites'', J. Am. Ceram. Soc. 88 (2005) 2354–2361.
[32] I. MacLaren, R.M. Cannon, M.A. Gülgün, R. Voytovych, N. Popescu-Pogrion, C. cheu, U. Täffner, M. Rühle, Abnormal grain growth in alumina: synergistic effects of yttria and silica, J. Am. Ceram. Soc. 86 (2003) 650–659.